

Experiments in a novel quasi-1D diffusion flame with variable bulk flow

E. Robert and P.A. Monkewitz

Laboratory of Fluid Mechanics (LMF), Swiss Federal Institute of Technology Lausanne (EPFL), CH-1015 Lausanne, Switzerland

Abstract

The novel species injector of a recently developed research burner, consisting of an array of hypodermic needles, which allows to produce quasi one-dimensional unstrained diffusion flames has been improved. It is used in a new symmetric design with fuel *and* oxidizer injected through needle arrays which allows to independently choose both the magnitude and direction of the bulk flow through the flame. A simplified theoretical model for the flame position with variable bulk flow is presented which accounts for the transport properties of both reactants. The model results are compared to experiments with a CO_2 -diluted H_2-O_2 flame and variable bulk flow. The mixture composition throughout the burning chamber is monitored by mass spectrometry. The resulting concentration profiles are also compared to the simplified theory and demonstrate that the new burner configuration produces a good approximation of the 1-D chambered diffusion flame, which has been used extensively for the stability analysis of diffusion flames. Hence, the new research burner opens up new possibilities for the experimental validation of theoretical models developed in the idealized unstrained 1-D chambered flame configuration, in particular models concerning the effect of bulk flow magnitude and direction on flame stability. Some preliminary results are presented on the effect of bulk flow direction on the thermal-diffusive cellular flame instability.

Keywords: Diffusion flame, unstrained, instability

1. Nomenclature

C_p	Specific heat at constant pressure	T_f	Adiabatic flame temperature
D_i	Diffusivity of species i	U	Bulk flow velocity
$Le_i = \kappa/D_i$	Lewis number of species i	\bar{W}	Mean molecular weight
q	Heat released per unit mass of fuel	W_i	Molecular weight of specie i
Q	Total heat released	X_f	Fuel mass fraction
		X_o	Oxidizer mass fraction
		x	Coordinate along burner length

$\kappa = \lambda/(\rho C_p)$	Thermal diffusivity
ν_i	Stoichiometric coefficient of species i
ρ	Density
ϕ	Equivalence ratio
ω	Chemical reaction rate

2. Introduction

In chemically reacting flows, instabilities arise from the competing mechanisms of thermal and mass diffusion. These thermo-diffusive instabilities can manifest themselves by cellular patterns in the reaction zone [1–4] which have been observed in non-premixed systems. In technological applications, they were found to play a significant role in soot formation and extinction dynamics [5].

Since its introduction by Kirkby and Schmitz [6], the idealized chambered flame model has been and continues to be used extensively to study the stability of diffusion flames in the absence of hydrodynamic effects [1–4, 7, 8]. The simplicity of this configuration, illustrated in figure 1a), allows for analytical solutions to the governing equations of the chemically reacting flow. Models developed in this configuration have the advantage of uncoupling thermo-diffusive instabilities from any hydrodynamics. However, until recently these models have remained without experimental validation because of the difficulty to realize such configurations experimentally.

The challenge arises from the necessity to supply the reactants and remove the products evenly across the burner cross section to maintain the one-dimensional character of the flame and avoid strain which has a strong effect on flame stability and extinction dynamics [9]. A novel research burner configuration has recently been introduced that creates such a flame [10, 11] by using an array of hypodermic needles to supply the reactants and allowing the products to escape between them. In this paper, a new improved symmetric version of this burner is presented in which both reactants are supplied through hypodermic needle arrays and the products can escape in both directions. By adjusting the ratio of products escaping on the fuel and oxidizer side, the investigation of the effect of bulk flow magnitude and direction on a one-dimensional unstrained diffusion flame is made possible. This configuration will in particular allow for the first time to create a planar flame with no net flow across the reaction zone, i.e. a flame where all mass transports are effected by diffusion only.

3. Theoretical model

We start from the simplified theoretical model for the idealized chambered diffusion flame of figure 1(a) (see e.g. Cheatham & Matalon [3]). In the original configuration, one reactant (usually the fuel) is supplied from the bottom with a uniform velocity \tilde{U} , while the oxidizer is introduced from the top and reaches the reaction area solely by diffusion against

the flow of products. The distribution of oxidizer and products is ‘magically’ kept uniform over the cross section by the fast top stream which removes combustion products and supplies reactant. In the following, this model is adapted to the more general symmetric configuration shown in figure 1(b) with arbitrary bulk flow velocity and direction.

3.1. Reaction-sheet approximation

In the new symmetric burner configuration, shown in figure 1(b), the fuel and oxidant are introduced uniformly over the burner cross section at $\tilde{x} = 0$ and $\tilde{x} = L$, respectively. In the following, dimensional variables and unscaled mass fractions X are designated by $\tilde{\cdot}$. It is assumed that both reactants follow Fick’s law of mass diffusion and burn in a global one-step irreversible reaction 1.



Next, we make the drastic assumption of constant density $\tilde{\rho}$ and transport properties D_i , κ and C_p , independent of temperature. In addition, it is reasonable to assume that both reactants and the combustion products have identical \tilde{W} , κ and C_p since both reactants are diluted with an inert (CO_2) that constitutes the bulk of the mixture. As a consequence of $\tilde{\rho} = \text{const.}$ the bulk flow velocity \tilde{U} becomes constant over the entire burner length. This simplifies the steady-state dimensional equations of conservation of species and energy to:

$$\tilde{\rho} \tilde{U} \frac{\partial \tilde{X}_o}{\partial \tilde{x}} - D_o \tilde{\rho} \frac{\partial^2 \tilde{X}_o}{\partial \tilde{x}^2} = -\nu_o W_o \tilde{\omega} \quad (2)$$

$$\tilde{\rho} \tilde{U} \frac{\partial \tilde{X}_f}{\partial \tilde{x}} - D_f \tilde{\rho} \frac{\partial^2 \tilde{X}_f}{\partial \tilde{x}^2} = -\nu_f W_f \tilde{\omega} \quad (3)$$

$$\tilde{\rho} C_p \tilde{U} \frac{\partial \tilde{T}}{\partial \tilde{x}} - \lambda \frac{\partial^2 \tilde{T}}{\partial \tilde{x}^2} = \tilde{Q} \tilde{\omega} \quad (4)$$

The system is made dimensionless using the chamber length L as characteristic length and κ/L as characteristic velocity. The reference temperature is \tilde{q}/C_p where $\tilde{q} = \tilde{Q} \tilde{X}_{f,L}/\nu_f W_f$ represents the heat released per unit mass of fuel consumed. The mass fractions of fuel and oxidizer, finally are scaled with the conditions where they are introduced: the fuel mass fraction by $\tilde{X}_{f,0}$ at $\tilde{x} = 0$ and the oxidizer mass fraction by $\phi \tilde{X}_{o,L}$ at $\tilde{x} = L$, where ϕ is the fuel-to-oxidizer equivalence ratio.

$$\phi = \frac{\tilde{X}_{f,L}/\nu_f W_f}{\tilde{X}_{o,0}/\nu_o W_o} \quad (5)$$

Invoking the large activation energy approximation, where it is assumed that no reaction occurs outside of a thin reaction sheet located at $\tilde{x} = \tilde{x}_f$, the dimensionless equations are obtained as

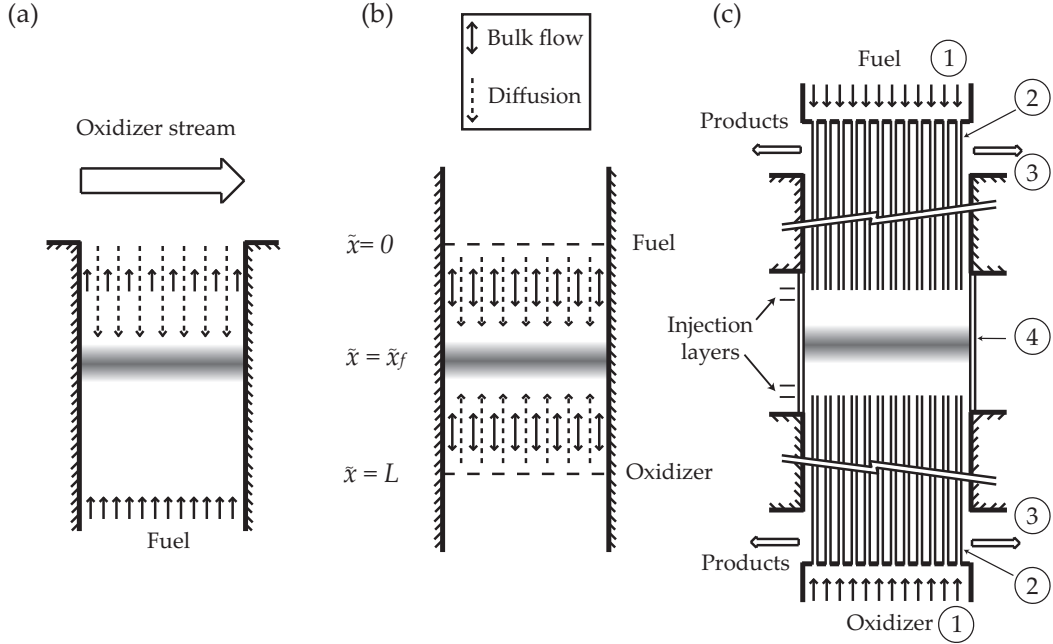


Fig. 1: a) Conventional chambered diffusion flame. b) Symmetric chambered diffusion flame with reversible bulk flow. c) Experimental configuration used. 1, Injection Plenum; 2, Array of hypodermic injection needles; 3, The products are allowed to escape between the injection tubes; 4, Quartz-walled reaction chamber.

$$U \frac{\partial X_o}{\partial x} - Le_o^{-1} \frac{\partial^2 X_o}{\partial x^2} = -\omega \delta(x - x_f) \quad (6)$$

$$U \frac{\partial X_f}{\partial x} - Le_f^{-1} \frac{\partial^2 X_f}{\partial x^2} = -\omega \delta(x - x_f) \quad (7)$$

$$U \frac{\partial T}{\partial x} - \frac{\partial^2 T}{\partial x^2} = \omega \delta(x - x_f) \quad (8)$$

where $\omega \delta(x - x_f) = \nu_f W_f L^2 \tilde{\omega}(\tilde{x}) [\kappa \tilde{\rho} \tilde{X}_{f,0}]^{-1}$. The non-dimensional boundary conditions at the location of fuel and oxidizer injection at $x = 0$ and $x = 1$, respectively are

$$x = 0 : \quad X_f = 1, X_o = 0, T = T_0 \quad (9)$$

$$x = 1 : \quad X_o = \phi^{-1}, X_f = 0, T = T_L \quad (10)$$

To link the solutions across the flame sheet at $x = x_f$, equations (6) - (8) are integrated from $x = x_f - 0$ to $x = x_f + 0$ to yield the jump conditions

$$[T] = [X_o] = [X_f] = 0 \quad (11)$$

$$\begin{aligned} \left[\frac{\partial T}{\partial x} + Le_o^{-1} \frac{\partial X_o}{\partial x} \right] &= \\ \left[\frac{\partial T}{\partial x} + Le_f^{-1} \frac{\partial X_f}{\partial x} \right] &= 0 \quad (12) \end{aligned}$$

where the operator $[\cdot]$ represents the jump of the respective quantity across the reaction sheet (the difference between its value at $x_f + 0$ and $x_f - 0$). These jump relations (11) and (12) represent respectively continuity of all variables and the fact that the reactants have to reach the flame sheet in stoichiometric proportions to have complete combustion, i.e. to satisfy the boundary conditions $X_o(x = 0) = 0$ and $X_f(x = 1) = 0$.

3.2. Model results

The above model corresponds to the leading order of the activation energy expansion of Cheatham [3], with slightly different boundary conditions resulting from the finite chamber length, and represents a stable planar flame sheet. Solving equations (6) - (8) in each sub-domain $0 \leq x \leq x_f$ and $x_f \leq x \leq 1$ and applying the boundary and jump conditions (9) - (12) yields the flame position x_f given by equation (13) and the species and concentration profiles (14) - (16), where T_f is the adiabatic flame temperature defined by the jump relation.

$$\frac{e^{-ULe_f x_f} - 1}{e^{ULe_o(1-x_f)} - 1} = -\phi \quad (13)$$

$$X_o = \begin{cases} 0 & \text{for } 0 \leq x \leq x_f \\ \frac{1}{\phi} \frac{e^{ULe_o x} - e^{ULe_o x_f}}{e^{ULe_o} - e^{ULe_o x_f}} & \text{for } x_f \leq x \leq 1 \end{cases} \quad (14)$$

$$X_f = \begin{cases} \frac{e^{ULe_f x} - e^{ULe_f x_f}}{1 - e^{ULe_f x_f}} & \text{for } 0 \leq x \leq x_f \\ 0 & \text{for } x_f \leq x \leq 1 \end{cases} \quad (15)$$

$$T = \begin{cases} \frac{(T_f - T_0)e^{Ux} + T_0 e^{Ux_f} - T_f}{e^{Ux_f} - 1} & \text{for } 0 \leq x \leq x_f \\ \frac{(T_f - T_L)e^{Ux} + T_L e^{Ux_f} - T_f e^U}{e^{Ux_f} - e^U} & \text{for } x_f \leq x \leq 1 \end{cases} \quad (16)$$

It is interesting to notice in equation 13 that the flame position in the present finite length burner depends on the Lewis number of *both* species, in contrast to the semi-infinite configuration of Cheatham [3] where x_f depends only on the Lewis number of the species which has to diffuse against the bulk flow.

In the limiting case of vanishing bulk flow $U = 0$, the expressions (13) - (16) have to be evaluated with Hôpital's rule to yield the limiting flame position

$$x_f(U = 0) = \frac{\phi Le_o}{\phi Le_o + Le_f} \quad (17)$$

and linear concentration and temperature profiles not shown here.

4. Experimental set-up

The main challenge when attempting to create an unstrained chambered flame is to supply the reactants and remove the products evenly across the reaction area. A novel way to address this problem and produce a truly unstrained flame has recently been successfully implemented [10, 11]. In this first implementation the reactant which has to diffuse against the bulk flow is introduced through an array of hypodermic needles between which the products can escape.

4.1. Burner description

In the present paper we introduce the symmetric 'Mark II' version of this novel research burner in which both reactants are introduced through needle arrays. A photograph of the partially assembled burner is shown in figure 2. The symmetric arrangement of the product extraction manifolds exhausting into two exhaust plenums on both ends (not shown on the photograph) allows control over both the magnitude and direction of the bulk flow through the flame by adjusting the pressure difference between the two exhaust plenums. A conceptual sketch of the burner is presented in figure 1(c). The injection arrays consist of $31 \times 31 = 961$ stainless steel hypodermic needles with an outer diameter of 1.2 mm and a wall thickness of 0.1 mm on a Cartesian grid with 2.5 mm spacing. Both arrays are introduced in a quartz walled burning chamber with a square cross-section of 77.5×77.5 mm². The products are allowed to escape through a second set of $32 \times 32 = 1024$

tubes of 1.2 mm I.D. located between the injection needles. These extraction tubes are bent outwards to deliver the exhaust gas into annular exhaust plenums which are heated to prevent condensation in the exhaust manifold resulting in non-uniform product extraction. The spacing between the two injection arrays is adjustable up to 80 mm, but for the present experiment it was always kept at 40 mm.

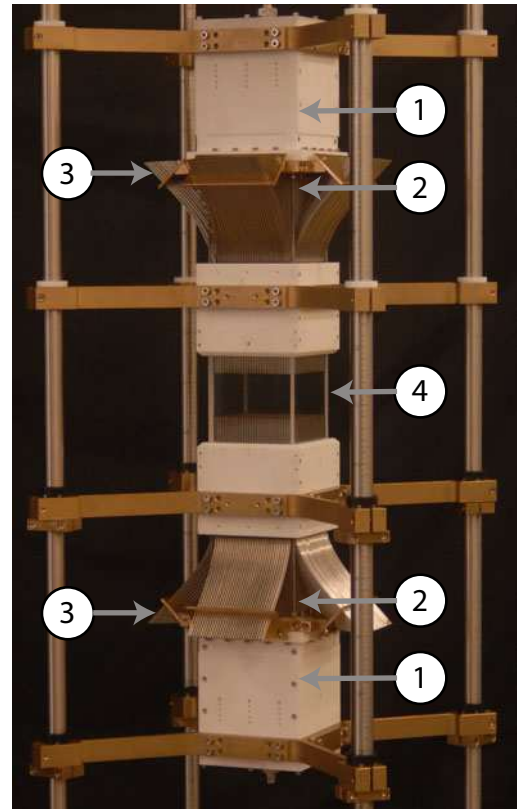


Fig. 2: Photograph of the partially assembled burner (without exhaust plenums and thermal insulation) with all needle arrays in place. 1, Reactant injection plenums; 2, Straight injection needle arrays emerging from plenums; 3, Extraction needles bent outwards between injection needles; 4, Quartz-walled reaction chamber.

While the injection of reactant through a discrete array of hypodermic needles is inhomogeneous close to the exit plane of the needles, it has been shown experimentally that this inhomogeneity disappears beyond an 'injection layer' of thickness comparable to the needle spacing. In the 'Mark I' version of the burner, the thickness of this three-dimensional injection layer has been measured in the 1.5 – 2.5 mm range [11], depending on flow velocities. Hence, the desired one-dimensional reactant transport is realized beyond the injection layers. For all the results presented here, the flame was always sufficiently outside of the injection layers to be one-dimensional over nearly the entire burner cross section. Weak inho-

mogeneities persist near the edges principally due to heat loss through the quartz windows of the burning chamber which are necessary to visualize the flame structure. This inhomogeneity over the burner cross-section is clearly visible when approaching extinction and results in rapid cell motion for cellular flames which complicates measurements. In the current version of the burner, this problem is alleviated by placing a quartz tube of 41 mm I.D., spanning the entire chamber length, between the two arrays of injection needles. This creates two separate flames, a uniform one in the center where the measurements are carried out and a surrounding annular flame that experiences significant gradients. From the experiments carried out in the Mark I version of the burner one can deduce that the residual strain experienced by the central flame is below 0.25 s^{-1} [11].

It is however clear that in our burner configuration a part of the reactant injected against the bulk flow turns around and is swept out of the burner, i.e. does not diffuse towards the flame. The determination of the effective species transport towards the flame therefore requires mass spectrometry.

4.2. Burner characterization

Mixture composition profiles taken between the two injection arrays were used to define the injection layer thickness, the effective boundary conditions and the mixture strength. Sampling was made through a fused silica capillary (0.2 mm outer diameter) progressively lowered through one of the exhaust tubes. The capillary was protected by a 0.4 mm outer diameter stainless steel tube to avoid loss of integrity as the tip approaches the flame. The sampling rate of 0.1 ml/min was low enough to induce only minimal flow perturbations. The samples were analyzed with a quadrupole mass spectrometer (MKS Instruments, model LM92 Cirrus). The position of the sampling point was determined by photographs taken through the chamber windows.

An elaborate calibration procedure allows simultaneous measurement of all four species present within the burner (H_2 , H_2O , O_2 , CO_2) over a wide range of mixture composition using a single set of calibration data. The relative error of these measurements is below 7% for the concentration range investigated here. The profiles presented in figures 3 and 4 were taken at the center of the burner cross section in the fuel advected and fuel counter-diffusing configurations, respectively. They are compared with the results expected from the simplified theory of Section 3. The close agreement between theoretical and experimental concentration profiles demonstrates that our experimental set-up is a good realization of a 1D chambered diffusion flame. A photograph of the stable flat flame corresponding to figure 3 is shown in figure 5. It is noted that the somewhat higher luminosity of the hypodermic needles ends near the center as seen in figure 5 cannot be directly associated with a nonuniform temperature distribution. The reason is that in

the center, the light intensity is a superposition of the “glows” from 31 rows of needles, since the camera is centered relative to the burner and sees right through the tube array. On the sides only the light emitted from the first few rows reach the camera because of the wide angle objective used, hence leading to an apparently brighter center.

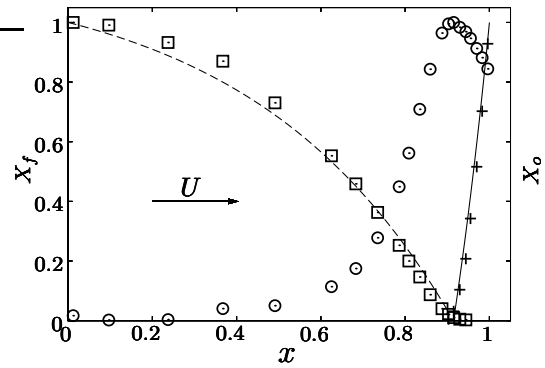


Fig. 3: Concentration profiles in the reaction chamber with fuel advected from the left ($x=0$) for $U = +7.05$ ($\tilde{U} = 0.044 \text{ m/s}$ with $\tilde{\rho}$ and κ evaluated at the adiabatic flame temperature of 1550 K), $\phi = 1$, $Le_f = 0.35$ and $Le_o = 0.86$. \square , experimental H_2 concentration X_f ; $- - -$, equation 15; $+$, experimental O_2 concentration X_o ; $-$, equation 14; \circ , experimental H_2O concentration.

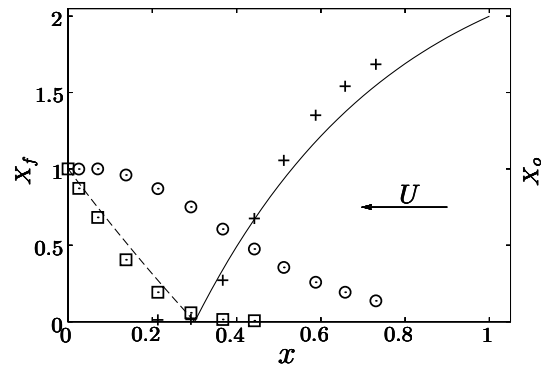


Fig. 4: Concentration profiles in the reaction chamber with fuel counter-diffusing from the left ($x=0$) for $U = -2.64$ ($\tilde{U} = -0.036 \text{ m/s}$ with $\tilde{\rho}$ and κ evaluated at the adiabatic flame temperature of 1370 K), $\phi = 0.5$, $Le_f = 0.25$ and $Le_o = 0.80$. Symbols are the same as in figure 3.

5. Experimental results

5.1. Flame position

To measure the flame location in the burner, photographs were taken from the side. The images



Fig. 5: Stable flat flame corresponding to figure 3. The fuel is supplied from the bottom and advected to the flame by the upward bulk flow. The white arrows indicate the diameter of the inner quartz tube inserted in the burner to separate the central region, where the flame is observed and probed, from the burner edges.

where then analyzed and the flame position determined as the point of maximum luminosity in the center of the chamber. This optically determined flame location was checked to be in excellent agreement with the location of the water concentration and temperature maxima. For the sake of simplicity, the optical method was used for the majority of the results presented here. For each experimental condition, the effective mixture composition immediately next to the injection needle array supplying the counter-diffusing species was measured by mass spectrometry. These local concentration profiles, extending from the injection tube tips to the flame, allowed the determination of the effective boundary condition at the edge of the downstream injection layer, i.e. the amount of reactant swept into the exhaust by the bulk flow, and hence the effective mixture strength in the burner. Based on this concentration profile, a point beyond the injection layer was chosen as the *virtual origin* of the counter-diffusing reactant. The mixture composition and temperature at this point were then used as boundary condition and the reduced chamber length as the new reference length for the comparison with the simplified model of section 3. This procedure allowed the effective mixture strength ϕ to be kept constant, despite the varying loss of counter-diffusing species into the exhaust at different bulk flow velocities.

A comparison between the measured flame position and the position calculated from equation 13 is presented in figures 6 and 7 and clearly shows the influence of bulk flow magnitude and direction. To evaluate the theoretical flame position, the experimental Lewis numbers of the reactant mixtures were taken at the advecting and counter-diffusing inlets, respectively. The dimensional experimental bulk velocity was determined from the mass flow and the mixture density evaluated at the upstream combustion chamber inlet temperature. The thermal diffusivity κ , to non-dimensionalize the bulk velocity, on the other hand, was evaluated at three different temperatures: at both inlet temperatures and at the adiabatic flame temperature determined with the Cantera software package [12, 13].

These results show good agreement between the simplified theory for the flame position (equation

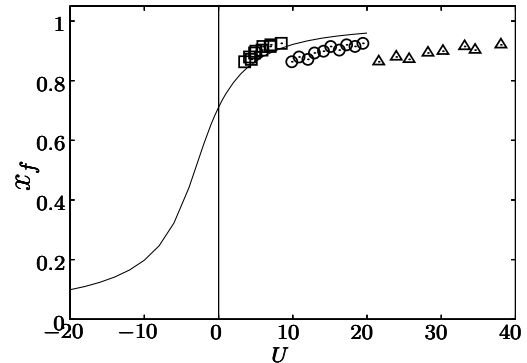


Fig. 6: Effect of bulk flow velocity on flame position for the case of counter-diffusing oxidant. The κ used to non-dimensionalize the bulk velocity is evaluated at the flame (\square), at the advecting inlet (\circ) and at the counter-diffusing inlet (\triangle). —, theoretical x_f for $\phi = 1$, $Lef = 0.35$ and $Le_o = 0.85$.

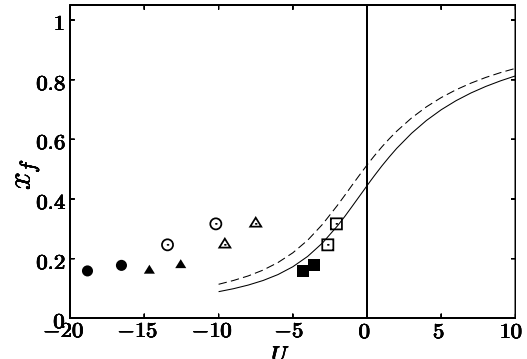


Fig. 7: Effect of bulk flow velocity on flame position for the case of counter-diffusing fuel with $\phi = 0.25$, $Lef = 0.25$ and $Le_o = 0.80$ (solid symbols and theoretical line) and $\phi = 0.33$, $Lef = 0.25$ and $Le_o = 0.80$ (open symbols and dashed theoretical line). The κ used to non-dimensionalize the bulk velocity is evaluated at the flame (\square , \blacksquare), at the advecting inlet (\circ , \bullet) and at the counter-diffusing inlet (\triangle , \blacktriangle).

13) and the experimental results. It clearly appears that the adiabatic flame temperature is the most appropriate temperature to evaluate κ for the non-dimensionalization of the bulk velocity. The figures also show that the flame position is more accurately predicted by the simplified theory when the oxygen rather than the hydrogen is counter-diffusing.

Several factors can be invoked to explain the differences between the two data sets. The assumption of constant transport properties made in the theoretical development is not equally drastic in both configurations. Equation (13) reveals that the flame position is mainly determined by the Lewis number of

the counter-diffusing species. In the present experiments, Le_o varied only slightly from the injection point to the flame sheet (from 0.861 to 0.865) when the oxidant was counter diffusing. When the fuel was counter-diffusing, the Le_f variation was more significant, between 0.25 at the injection and 0.22 at the flame, on average. In addition, the thermal expansion, also neglected in the simplified theory, decreases the transport of the counter-diffusing species to the reaction zone. This effect increases the effective ϕ when the oxidant is counter-diffusing and decreases it in the reverse configuration (note that a decreasing ϕ lowers the curve $x_f(U)$ in figures 6 and 7).

5.2. Flame stability

The stable flame sheet is rendered unstable by slowly lowering the hydrogen concentration in the fuel stream. When approaching the lean extinction limit, the stable flame sheet fragments into cells. The asymptotic theory of diffusion flames [3, 4] predicts that a cellular flame pattern forms near extinction if the reactants Lewis numbers are sufficiently small. Examples of cellular flames are shown in figure 8 for the two cases of counter-diffusing oxidant and fuel. As mentioned previously, a quartz tube of 41 mm I.D., seen in figure (8a), was inserted between the two injection arrays to separate the central region with extremely low strain from the edges of the burner where temperature gradients resulting from heat loss through the burner walls are more significant.

The introduction of the quartz tube in the chamber allows for easy measurement of the cell size. In the advected fuel configuration of figure (8b), there are 11 cells aligned along the inner tube perimeter, yielding a cell size of about 9.1 mm. When the oxidant is the advected species, as in figure (8c), only 6 cells are visible yielding a wave length of about 14 mm.

The scaling of the cell size has been addressed in stability analyzes of cellular diffusion flames [1, 3]. To compare the two cellular flames of figure (8), the problem of where to evaluate the transport properties arises. Here they are assumed equal in the two configurations since at the flame the mixture consists only of inert and products, with vanishingly small concentrations of reactants. In both of the references cited above, the cell size is found to scale with $1/\tilde{U}$ when all mixture properties are held constant. Considering the (drastic) model assumptions, this scaling appears to be confirmed by the present preliminary experiments which produce a cell size ratio of 1.55 for a ratio of bulk velocity magnitude of 1.4. The evaluation of the scaling of cell size with reactant properties, i.e. the evaluation of the pre-factor of $1/\tilde{U}$, on the other hand, and the investigation of a wider range of bulk velocities including the limit $\tilde{U} \rightarrow 0$ will be the subject of future experiments.

6. Conclusions

The burner presented in this paper has evolved

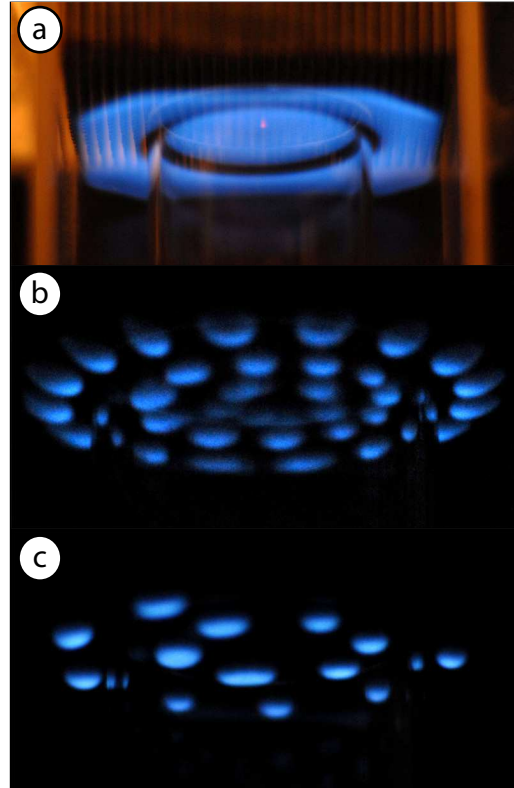


Fig. 8: Low angle view (-30°) of the burner used to capture the flame structure. (a) Reference view of stable flame, with the central quartz tube visible; (b), cellular flame with advecting fuel ($\tilde{U} = 0.036$ m/s); (c), cellular flame with counter-diffusing fuel ($\tilde{U} = -0.026$ m/s).

from the first experimental realization of a 1D chambered diffusion flame [10, 11]. The novel symmetric design of the reactant supply to the burning chamber allows the investigation of the effect of bulk flow magnitude and direction on a diffusion flame in the absence of strain. This design is in particular aimed at the first investigation of a purely diffusive unstrained flame in the zero bulk flow limit. The practical difficulty with this design due to the unknown proportion of fuel and/or oxidant lost into the exhausts has been overcome by the systematic use of mass spectroscopy in the burner chamber. The key to the successful use of the mass spectrometer in this situation with large concentration variations is an innovative calibration procedure [11] which yields continuous concentration profiles of the 4 species present in the burner and permits the determination of the effective mixture strength of the flame.

The good agreement between the present experiments and the simple theory for the flame position and the species concentration profiles demonstrates that our new symmetric burner is a good approximation of a chambered one-dimensional diffusion flame, with one species transported against the bulk flow by

diffusion only. Preliminary observations of cellular flame patterns for both the advected fuel and counter-diffusing fuel configurations are compatible with a cell size scaling proportional to $1/\tilde{U}$ when all the transport properties are held constant.

The authors wish to express their gratitude for the support received from the Swiss National Science Foundation under Grant 20020-108074.

References

- [1] J. S. Kim, F. A. Williams, P. D. Ronney, *J. Fluid Mech.* 327 (1996) 273–301.
- [2] J. S. Kim, *Combust. Theory Modelling* 1 (1997) 13–40.
- [3] S. Cheatham, M. Matalon, *J. Fluid Mech.* 414 (2000) 105–144.
- [4] P. Metzner, M. Matalon, *Combust. Theory Modelling* 10 (4) (2006) 701–725.
- [5] J. S. Kim, F. A. Williams, *J. Engineering Mathematics* 31 (1997) 101–118.
- [6] L. L. Kirkby, R. A. Schmitz, *Combustion and Flame* 10 (3) (1966) 205–220.
- [7] C. K. Law, *Combustion physics*, Cambridge university press, 2006.
- [8] I. Glassman, *Combustion*, 3rd Edition, Academic Press, 1996.
- [9] C. L. Chen, S. H. Sohrab, *Combustion and Flame* 86 (1991) 383–393.
- [10] D. Lofacono, P. Papas, M. Matalon, P. A. Monkewitz, *Proc. of the Combustion Inst.* 30 (2005) 501 – 509.
- [11] E. Robert, P. A. Monkewitz, in: *5th US Combustion Meeting*, San Diego CA, 2007.
- [12] D. G. Goodwin, Vol. 2003-08, The Electrochemical Society, p. 155–162.
- [13] D. G. Goodwin, *Cantera: Object-Oriented Software for Reacting Flows*, available at <http://www.cantera.org>.